Applied Catalysis B: Environmental 117–118 (2012) 156–166

Contents lists available at SciVerse ScienceDirect

Applied Catalysis B: Environmental

journal homepage: www.elsevier.com/locate/apcatb

Structural investigation of $LaCoO_3$ and $LaCoCuO_3$ perovskite-type oxides and the effect of Cu on coke deposition in the partial oxidation of methane

Fabio Souza Toniolo, Robert Newton S.H. Magalhães, Carlos André C. Perez, Martin Schmal*

Federal University of Rio de Janeiro, Chemical Engineering Program, NUCAT/PEQ/COPPE – Centro de Tecnologia, Bl. G 128, C.P. 68502, CEP. 21941-914 Rio de Janeiro, Brazil

ARTICLE INFO

Article history:
Received 20 September 2011
Received in revised form
16 December 2011
Accepted 6 January 2012
Available online 16 January 2012

Keywords:
Perovskite
Partial oxidation
Copper
Coke inhibition
Methane

ABSTRACT

$LaCoO_3$ and $LaCo_{0.8}Cu_{0.2}O_3$ perovskite-type oxides prepared by the polymerizable complex route were obtained as single phase and investigated in the partial oxidation of methane through temperature-programmed surface reactions (TPSR). Characterizations were carried out before and after the reactions under different feed streams $CH_4/O_2/He = 2/1/37$ and $5/1/64$, and revealed a dynamic structural transformation in which the perovskite is collapsed towards lanthanum-based matrix and metal cobalt and copper. The copper-substituted perovskite showed better performance in the partial oxidation of methane leading to higher CH_4 conversion and higher syngas production than $LaCoO_3$ during the transient reaction. Furthermore, copper had significant effect against carbon deposition on the catalyst and it is suggested to be a very important dopant for perovskites applied in reactions with hydrocarbons.

1. Introduction

Perovskite-type oxides with structure ABO_3 have attracted significant interest in many areas of solid-state chemistry, including catalysis. These complex oxides can be properly modified by the partial substitution of atoms at A and/or B sites, which may affect strongly the catalytic activity due to stabilization of unusual oxidation states of the B component, as well as the formation of structural defects [1]. From the catalysis point of view, perovskite-type oxides enable the generation of catalysts with active metals finely dispersed onto a matrix produced *in situ* from an oxide precursor [2–4]. High metal dispersion from perovskite emerges as a practical alternative and can be applied in the partial oxidation of CH_4 (POM). According to Slagtern et al. [5], when $LaCoO_3$ perovskite was tested in the POM, this catalyst became active to produce H_2 and CO due to the formation of disperse Co^0 onto a La_2O_3 matrix. The combined reforming of methane with CO_2 and O_2 for syngas production using $LaCoO_3$ perovskite showed good performance to H_2 and CO [3]. However other investigations with $LaCoO_3$ in the POM have evidenced low CH_4 conversion and low selectivity to syngas due to the reoxidation, during the reaction, of cobalt previously reduced [6,7].

Recently $LaNiCoO_3$ perovskites were used as catalyst precursors in the POM and the substitution of Ni by Co caused an increase in the reduction temperature, which can be associated with the metal–metal interactions during the reduction process [8]. Particularly, $LaCoO_3$ perovskite is an attractive oxide since it is very reducible and presents a rich behavior in phases under reducing conditions, which can be significantly influenced by the incorporation of other metals into the perovskite structure [9]. Ruthenium-substituted $LaCoO_3$ perovskites have been investigated by Mota et al. [10] as precursors of catalysts in the oxidative reforming of diesel for hydrogen production and the results revealed that the increase in Co substitution by Ru led to a better reducibility, smaller particle size of La_2O_3 and Co^0 phases and better surface concentration of Ru^0 particles, which directly affected the catalytic behavior: the greater $Co^0 + Ru^0$ exposition and the higher extension of the $La_2O_2CO_3$ phase derived from perovskites then the higher activity and stability of the catalysts. Another system based on doping $LaCoO_3$ with copper showed that the presence of this metal increased the reducibility and also promoted a strong Co–Cu interaction able to increase the cobalt dispersion and avoid the copper sintering [11]. ZrO_2-supported $LaCoO_3$ with small perovskite grain size and small $LaCoO_3$ crystallites has been found to be very active and stable for hydrogen production by oxidative reforming of diesel, even at very high space velocities, showing ability to be scaled-up for use in diesel reformers [12].

Lanthanum cobaltite materials as powder catalysts may be synthesized by different techniques including solid-state reactions based on oxides, carbonates and oxalates of metal components; thermal decomposition of precipitated precursors as well as combustion of precursors. However, according to Popa and Kakihana

* Corresponding author.
E-mail address: schmal@peq.coppe.ufrj.br (M. Schmal).

0926-3373/$ – see front matter © 2012 Elsevier B.V. All rights reserved.
doi:10.1016/j.apcatb.2012.01.009

[13] the development of new methods has tried to improve the synthesis conditions in order to obtain pure phases at lower temperatures, besides preparing finer and homogeneous powders. The synthesis of $LaCoO_3$ using a simple Pechini-method assigned as polymerizable complex route, which is based on polyesterification between citric acid (CA) and ethylene glycol (EG) was first reported and investigated by these authors [13] and proved to achieve an easy control over the final stoichiometry, low processing temperature without intermediate grinding, high homogeneity of the resulting material and single-phase perovskite powders with high-surface area [13,14]. Kumar et al. [15] also observed the synthesis employing citric acid and ethylene glycol led to perovskite powders with finer size, more uniform morphology, higher porosity and lesser tendency to agglomeration than materials synthesized by co-precipitation and combustion method.

This article deals with the synthesis of $LaCoO_3$ and $LaCoCuO_3$ perovskites by the polymerizable complex method and investigates their structural modifications resulting from temperature-programmed surface reactions (TPSR) in the partial oxidation of methane for syngas production, as well as the effect of copper substitution on the catalytic performance. The perovskite-type oxides were characterized before and after TPSR experiments in order to elucidate the structural changes of the catalysts.

2. Experimental

2.1. Preparation of catalysts

Perovskites were prepared by the polymerizable complex route, which is based on the polyesterification between citric acid (99.5% minimum, Vetec) and ethylene glycol (99.5% minimum, Vetec) [13]. Solutions from the nitrate precursors $La(NO_3)_3{\cdot}6H_2O$ (99% minimum, Vetec), $Co(NO_3)_2{\cdot}6H_2O$ (98% minimum, Vetec) and $Cu(NO_3)_2{\cdot}3H_2O$ (99% minimum, Vetec) were prepared to give 0.4 mol L^{-1} and those ones containing the metal of interest were added in appropriate amount into a solution of CA 1.0 mol L^{-1} to satisfy the molar ratio of total metals and CA 1:1. The mixture was stirred for 30 min at 90 °C on a thermal plate to form stable metal complexes, then ethylene glycol was added in the molar ratio CA:EG = 3:2 to allow the polyesterification of the metal complexes. A polymeric resin was obtained after some hours in constant stirring and heating and then heat-treated into two steps: the first calcination performed at 450 °C/2 h in air to eliminate organic constituents and the second at 900 °C/3 h in air to generate a pure phase metal oxide.

2.2. Characterization of catalysts

The chemical composition of the catalysts was determined by X-ray fluorescence (XRF) in a Rigaku model RIX 3100 equipment with the samples under pellet form. The BET specific area was evaluated by nitrogen adsorption isotherms at −196 °C using an apparatus ASAP-2020 (Micromeritics®). Prior to this analysis, the samples were degassed at 300 °C overnight.

The X-ray powder diffraction measurements were performed using Rigaku DMAX 2500 PC diffractometer operated at 40 kV and 40 mA, using the graphite monochromated Cu Kα radiation. The diffractograms were recorded over 2θ values ranging from 10 to 80° with a scanning rate of 1 s/step and 0.05 step size. The diffraction data were refined by means of Rietveld method using FullProf Suite® software package and graphical interface WinPLOTR (this methodology is based on the simulation of the entire diffractometric pattern using structural parameters of the constituent phases). Lattice parameters of the perovskite phase were determined by the refinement, while mean crystallite size was calculated by Scherrer's equation using the values of the full-width at half-maximum (FWHM) of the peak referent to the plane (*h k l*) specified in Table 2.

Sample images were recorded in a field emission gun scanning electron microscope FEG-SEM (FEI Company) model QUANTA 400 without treatment. The sample was also investigated by transmission electron microscopy (TEM) in a JEOL equipment model JEM-1210, operating at 113–115 kV and equipped with Olympus Megaview G2 camera. The sample was first dispersed in isopropyl alcohol using ultrasonic bath for 10 min, then a small amount of this solution was dropped on a copper grid and dried before analysis.

Temperature programmed reduction (TPR) was performed with 50 mg of sample placed in a quartz microreactor coupled to a quadrupole mass spectrometer (Balzers-Pfeiffer). The pretreatment consisted in dehydrating the powder at 300 °C for 1 h in He flow 50 $cm^3\,min^{-1}$ prior the reduction. After cooling to room temperature the gas mixture was switched to 10 vol.% H_2/He at 50 $cm^3\,min^{-1}$ and the sample was heated up to 650 °C at 10 °C min^{-1} and kept at this temperature for 1 h. Calibration with CuO powder was performed to quantify the reduction degree of the samples.

Hydrogen chemisorption was carried out in order to obtain cobalt metal surface area and metal dispersion. The measurements were obtained with an apparatus model ASAP-2020 (Micromeritics®). Before H_2-chemisorption, *ca.* 500 mg of each sample was evacuated at 300 °C/30 min, cooled to room temperature and reduced in a 10 vol.% H_2/Ar flow under heating rate of 10 °C/min up to 650 °C, remaining at this temperature for 30 min. Then the sample was cooled to 400 °C and evacuated for 1 h at 1.0×10^{-6} Torr, and again cooled to 150 °C, which was the temperature of H_2 adsorption isotherm, varying the pressure from 50 to 515 Torr. The first isotherm represented the total amount of H_2 adsorption and the second one the reversible physisorbed hydrogen. The total H_2 uptake (μmol H_2 per gram of cobalt) was determined by extrapolation to null pressure. The adsorption stoichiometry was H/Co = 1/1, the percentage dispersion (*%D*) was calculated according to [16] and the metal specific area (S_m) as follows:

$$S_m = \frac{2 \times 10^{-6} \times H_T \times N_A}{N_S}\ [\mathrm{m^2\ per\ gram\ of\ cobalt}]$$

where H_T = total H_2 uptake ($\mu mol/g_{Co}$), N_A = Avogadro constant and $N_s = 1.51 \times 10^{19}$ atoms Co/m^2. It must be emphasized that the total-H_2 isotherm was employed to calculate the cobalt dispersion and metal specific area and not the irreversible chemisorption one (which is normally obtained by the difference between the total and reversible isotherms). The use of total H_2 uptake is adopted in the literature since the H_2-chemisorption over cobalt is usually activated (at 150 °C) [4,16–18].

After reaction, catalysts samples were analyzed by Raman spectroscopy at room temperature in spectrometer LabRam HR-UV800/Jobin-Yvon equipped with He–Ne laser (λ = 632 nm) of intensity 5.5 mW, charge-coupled device detector (−70 °C), Olympus BX41 microscope, objective lens of 100× and spot 0.96 nm (from 3 to 5 regions were analyzed in each sample). Thermogravimetric and differential analysis (TG-DTA Rigaku Thermo Plus TG8120) were carried out in 20% O_2/N_2 flow, heating rate of 10 °C/min from room temperature up to 1000 °C and using alumina as reference, in order to quantify carbon on the catalysts after reaction.

2.3. Catalytic evaluation

Temperature-programmed surface reactions were carried out in a fixed-bed U-shaped quartz reactor (12 mm i.d.) loaded with 100 mg of pure catalyst (no dilution with inert) under

Table 1
Investigated catalysts and results of chemical composition.

Catalyst	Codification	Calculated formula assuming O_3[a]	Real (nominal) content (wt.%)		
			La	Co	Cu
$LaCoO_3$	LC	$La_{1.02}CoO_3$	59.2 (56.5)	24.1 (24.0)	–
$LaCo_{0.8}Cu_{0.2}O_3$	LCCu	$La_{1.03}Co_{0.79}Cu_{0.21}O_3$	58.7 (56.3)	19.1 (19.1)	5.5 (5.2)

[a] Oxygen was not analyzed.

atmospheric pressure. A thermocouple was placed in contact with the reactor in order to measure the temperature. The total feed flow was held constant at 50 $cm^3\,min^{-1}$ (30 000 $cm^3\,g^{-1}\,h^{-1}$) and different mixtures were investigated $CH_4/O_2/He = 2/1/37$ and $CH_4/O_2/He = 5/1/64$. Dilute flows were employed owing to the sensitive filament of the mass spectrometer (Balzers-Pfeiffer) used to analyze all of the compounds from reaction.

The TPSR tests were performed as two consecutive runs described as follows: (i) reaction mixture flowed through catalytic bed at heating rate of 10 °C/min, from room temperature up to 900 °C, isothermal at 900 °C for 20 min; after this first run, the reactor was cooled up to 300 °C under the same mixture (ii) the second run was performed from 300 to 900 °C, 10 °C/min remaining isothermal at 900 °C for 20 min. Previous calibration was performed in order to correlate compounds concentration *versus* signal intensity, leading to a linear correlation for each compound. Such a procedure allowed obtaining quantitative data from temperature-programmed surface reactions, since frequent recalibrations were carried out to guarantee correct correlation between intensity and concentration. No pretreatment (*e.g.*, drying or reduction in H_2) was carried out because previous experiments showed that all the adsorbed water was released up to 200 °C during the first TPSR run, *i.e.*, before CH_4 and O_2 started reacting. Furthermore, any reduction pretreatment with H_2 was annulled in the first TPSR run between 160 and 310 °C, in which there was reoxidation of the metallic particles previously reduced in H_2. That is why all of the TPSR shown in this work were initiated directly with the reaction mixture.

The selectivity was defined as follows, where n_i represents the number of moles of the component and $\sum n_i$ the sum of moles of the products.

$$S(\%) = \frac{n_i}{\sum n_i} \times 100$$

3. Results and discussion

3.1. Characterization

The results of chemical composition for the catalysts are shown in Table 1 with the respective codification adopted from now on. The polymerizable complex route allowed achieving the desired stoichiometry, leading to similar nominal and real metal proportions. The perovskite LCCu presented lower cobalt content than LC because of the partial substitution of cobalt by copper. The XRD patterns of the catalysts after synthesis (Fig. 1) showed high crystallinity and only the perovskite phase was identified in both LC and LCCu samples (all of the diffraction peaks in the diffractograms refer to $LaCoO_3$ JCPDS 48-0123).

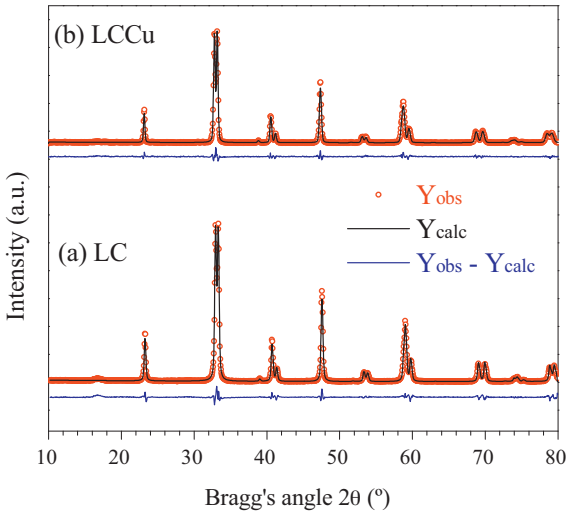

Fig. 1. Diffractograms and Rietveld refinement of the LC (a) and LCCu (b) perovskites. Y_{obs} symbols represent the experimental data, Y_{cal} line indicates the calculated curve and the difference between these data constitutes the blue line. (For interpretation of the references to color in this figure legend, the reader is referred to the web version of the article.)

The Rietveld refinement displayed very good correspondence between experimental data and the simulated curve (as seen in Fig. 1) and did not indicate the presence of any copper-segregated phase in LCCu, suggesting that Cu cations occupied sites in the crystalline perovskite structure. Moreover, this partial substitution is evidenced by the increase in cell parameters (see Table 2) caused by the difference in ionic radii of these metals, since the radius of hexacoordinated Cu^{2+} (its situation into B-site) corresponds to 0.73 Å which is larger than radius of Co^{3+} in the same position, 0.61 Å [19]. In the literature, similar observations have been reported [11,20]. The crystallite sizes for LC and LCCu were estimated in 45.0 and 55.6 nm, respectively. These big values are ascribed to the high calcination temperature (900° C) that causes sintering.

Textural properties of interest, *i.e.*, specific surface area, pore volume and average pore diameter are shown in Table 3. According to these data, the BET area is lower than 10 $m^2\,g^{-1}$. The adsorption and desorption isotherms (not shown here) are typical of macroporous solids (type II), in which the formation of N_2 monolayer adsorbed occurs at low relative pressures, followed by multilayers formation at higher pressures. However, the BJH pore diameter distribution was found to be heterogeneous with a sharp peak around 2.5 nm and another very broad between 20 and 90 nm.

Table 2
Crystallographic parameters and mean crystallite size of the samples studied.

Catalyst	Phase	Cell parameters (Å)			L_{hkl} [b] (nm)
		a	*b*	*c*	
LC	Perovskite[a]	5.43681	5.43681	13.10126	$L_{012} = 45.0$
LCCu	Perovskite[a]	5.45960	5.45960	13.14941	$L_{012} = 55.6$

[a] Phase identified in the literature as JCPDS 48-0123 ($LaCoO_3$).
[b] Mean crystallite size estimated with Scherrer's equation for the peak referent to the crystallographic plane *h k l*.

Table 3
Textural properties and H_2-chemisorption data of the perovskites.

Catalyst	Average pore diameter (BJH) (Å)	Mesopore volume (BJH) ($cm^3\ g^{-1}$)	Specific surface area (BET) ($m^2\ g^{-1}$)	Total H_2 uptake ($\mu mol/g_{Co}$)	S_m (m^2/g_{cat})
LC	166	0.015	<10	78	6.2
LCCu	82	0.0015	<10	152	12.1

According to Leofanti et al. [21] mesopores are between 2 and 50 nm and macropores are larger than 50 nm. Therefore, the catalysts have both mesopores and macropores, which is consistent with the BJH pore diameter.

SEM was an important tool to study the morphology and microstructure of the catalysts after synthesis and after catalytic evaluation. Micrographs of LC catalyst showed the presence of macropores (Fig. 2a) as indicated by N_2 physisorption results. These cavities result from the rearrangement of the solid while volatile materials are removed in the calcination steps. In Fig. 2b one can visualize the microstructure and the presence of grains ranging from 30 to 200 nm. There is an agglomeration tendency due to the high calcination temperature employed, although some grains with similar size obtained by XRD, *i.e.*, 45.0 nm, can be seen. Grains larger than 45.0 nm are polycrystals resulting from the sintering of many crystallites during calcination. Popa and Calderon-Moreno [14] studied the synthesis of $LaCoO_3$ by the polymerizable complex route and showed that a nucleation of single crystallites takes place between 400 and 450 °C after combustion of organics present in the amorphous precursor. After heating treatments at 700 and 900 °C, these authors verified clearly by HRTEM (high-resolution transmission electron microscopy) effects related to grain boundaries, dislocations networks, sintering and grain growth.

The micrographs of LCCu perovskite in Fig. 2c and d show morphology and microstructure similar to LC, with some grains reaching 300 nm of diameter. Tendency to agglomerate and form large cavities can be also seen in Fig. 2c. According to Kumar et al. [15], sol–gel methods lead to perovskites with fine and uniform grains, higher porosity and lower tendency to agglomeration than other methods under the same temperatures, such as coprecipitation and combustion. Concerning the influence of copper on the morphology and microstructure, nothing can be stated, because the calcination conditions appear to be definitely more relevant.

The H_2-TPR results showed similar profiles for LC and LCCu consisting in two peaks as displayed in Fig. 3. The first reduction peak centralized at 419 °C and 356 °C for LC and LCCu, respectively, is ascribed predominately to the reduction of Co^{3+} to Co^{2+} agreeing with the amount of H_2 associated to the area under this peak, which suggests total reduction Co^{3+}/Co^{2+}, however formation of Co^0 cannot be discarded. The second peak with maximum at 572 °C and 508 °C (LC and LCCu, respectively) is attributed to the reduction Co^{2+}/Co^0 and the quantitative analysis obtained from the area under the peaks suggests a reduction degree of 100% and 130% for LC and LCCu, respectively. The excessive H_2 consumption detected for the copper-substituted perovskite reflecting in a reduction degree higher than 100% indicates a phenomenon of H_2

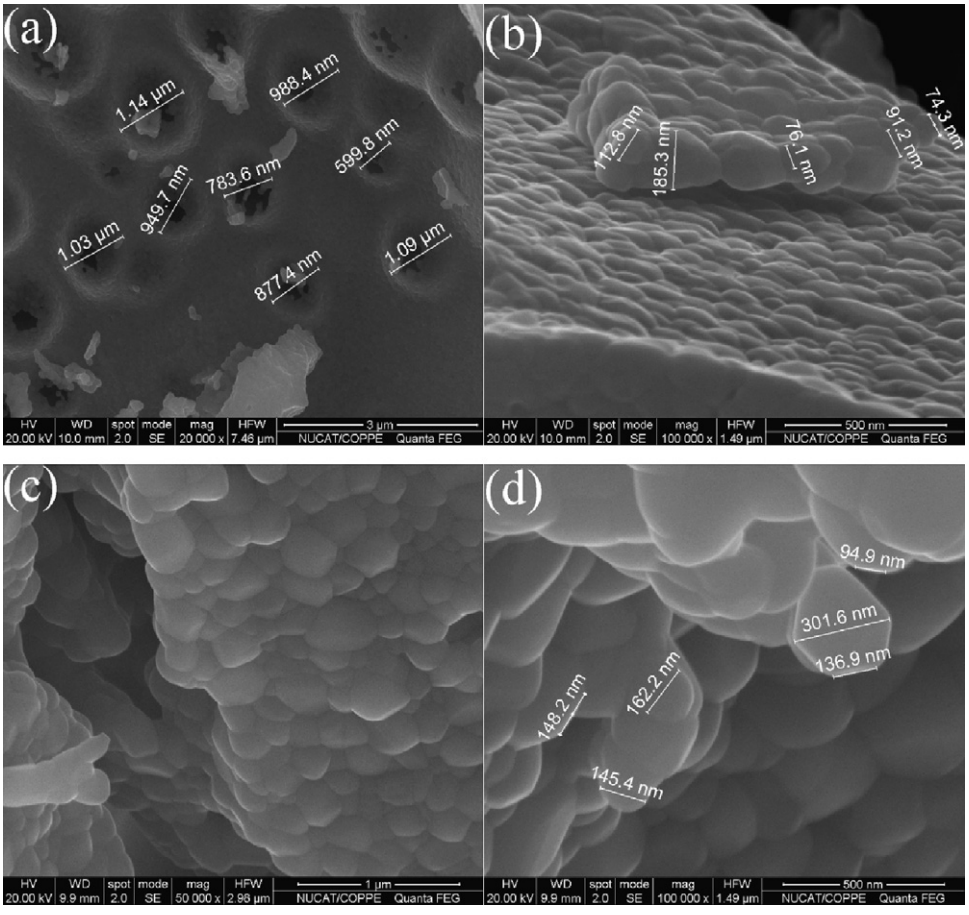

Fig. 2. SEM micrographs of the as-prepared LC (a, b) and LCCu (c, d) catalysts synthesized by the polymerizable complex route and calcined at 900 °C.

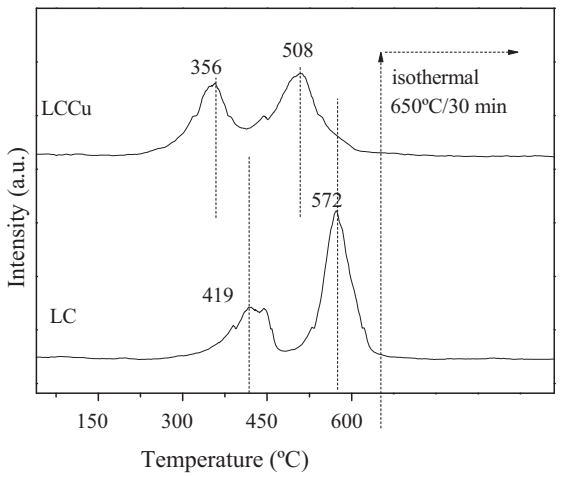

Fig. 3. H_2-TPR profiles of the as-prepared perovskite catalysts LC and LCCu (10%H_2/He, 10 °C/min).

spill-over. The reduction behavior observed for these perovskites are consistent with other results reported in the literature [4,11,22]. An important remark observed from the TPR profiles is that the presence of Cu shifts by approximately 60 °C the reduction profile, suggesting that Cu particles may catalyze the reduction of Co in the perovskite structure.

Concerning the H_2 chemisorption results shown in Fig. 4 and Table 3 for the catalysts after reduction procedure (therefore guaranteeing complete reduction), one can notice that total H_2 uptake doubled on the sample with Cu, which suggests higher cobalt dispersion on the surface promoted by Cu, since Cu does not adsorb H_2 under such conditions [23]. The cobalt metal areas are 6.2 and 12.1 m^2/g_{Co} for LC and LCCu, respectively, therefore the presence of Cu evidences strong cobalt–copper interaction that after reduction enhances the dispersion of Co particles. The metal dispersion is apparently low and estimated in 1% and 2% for LC and LCCu, which is explained due to the high cobalt content in the perovskites (24.1 and 19.1 wt.%, respectively) when compared to metal content on supported catalysts. Silva et al. [18] for instance, obtained cobalt dispersion between 0.84 and 7.1% for 5 wt.% Co/Nb_2O_5 when reduction degree was 100%; Reuel and Bartholomew [16] achieved cobalt dispersion in the range of 6.6–34% for 3, 10 and 15 wt.% Co/Al_2O_3 with reduction degrees <44%. It is important to emphasize that though the metal dispersion values are apparently low for LC and LCCu perovskites, the order of magnitude for H_2 total uptake is in perfect accordance to the literature [4,16–18] and does not represent low H_2 chemisorption. Echchahed et al. [4] obtained total H_2 uptake equivalent to 145 $\mu mol/g_{Co}$ for $LaCoO_3$ perovskites, which is very similar to LCCu.

3.2. Catalytic evaluation

LC and LCCu perovskites were tested in transient experiments in the partial oxidation of methane (POM) with $CH_4/O_2/He = 2/1/37$ and another more reducing mixture $CH_4/O_2/He = 5/1/64$, which is more prone to carbon deposition. The TPSR profiles obtained in the consecutive first and second runs for both catalysts are shown in Fig. 5. The blank test (no catalyst in the reactor) indicated that under $CH_4/O_2/He = 2/1/37$ there was some CH_4 conversion (~15%) only at the isothermal plateau at 900° C, while under $CH_4/O_2/He = 5/1/64$ no significant conversion was identified throughout the entire temperature range studied, indicating that the phenomena observed for LC and LCCu are catalytic and not due to thermal effects.

Concerning LC profiles in the POM $CH_4/O_2/He = 2/1/37$ (Fig. 5a), there is predominance of total oxidation of methane ($CH_4 + 2O_2 \rightarrow CO_2 + 2H_2O$) up to *ca.* 900 °C for both runs (first run = solid lines, second run = dashed ones), *i.e.*, fraction of CH_4 and total O_2 are converted to give water twice as carbon dioxide, as one can confirm in the profiles (~650–900 °C). The ratio $CH_4/O_2 = 2/1$ is suitable for the partial oxidation ($CH_4 + ½O_2 \rightarrow CO + 2H_2$); however, if total oxidation takes place ($CH_4 + 2O_2 \rightarrow CO_2 + 2H_2O$) then O_2 becomes a limiting reactant and CH_4 is in excess by a factor of 4, which may occur in the temperature range specified above. Noteworthy is that in the consecutive TPSR runs the second run evidences higher activity leading to reactions that started at lower temperatures. This activation phenomenon probably occurs owing to the structure reduction that took place in the first run at high temperature. The LCCu behavior (Fig. 5b) was similar to LC, however the total oxidation is reduced in approximately 100 °C, and, thus H_2 and CO become important syngas products above 800 °C, especially in the second run.

The catalytic evaluation of LC and LCCu in the POM $CH_4/O_2/He = 2/1/37$ showed that syngas arises only at high temperatures, but LCCu is able to produce syngas at temperatures lower than LC above ~750 °C. Besides, H_2 concentration attains 5% in the second run at 900 °C for the copper-substituted catalyst (and $H_2/CO = 2.1$), in opposition to LC which attains 0.8% of H_2 at the same conditions (only over time at 900 °C LC reaches relevant H_2 and CO concentrations). The Fig. 6 (black lines) exhibits that CH_4 conversion for LCCu in the second run increases from 29% to 68% at the temperature range 630–900 °C, which is superior to CH_4 conversion obtained with LC in the same range. Table 4 summarizes the catalytic results at different temperatures and indicates that during

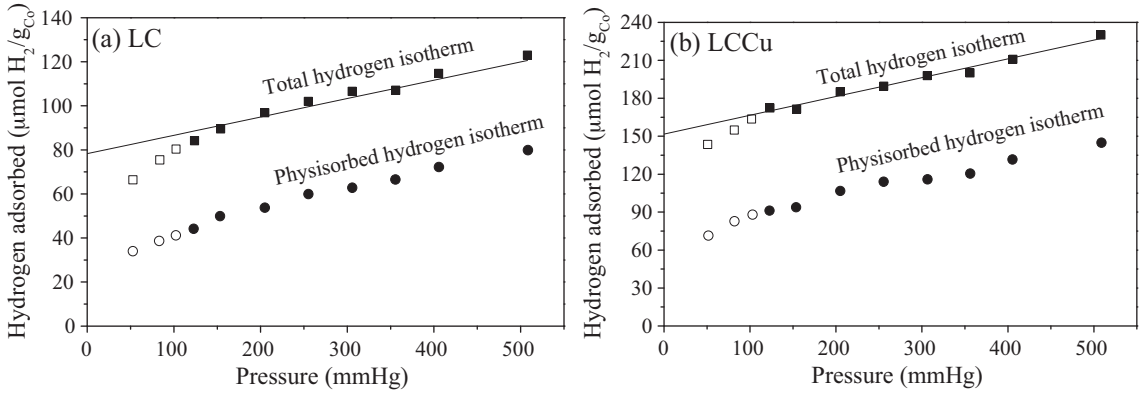

Fig. 4. Hydrogen adsorption amount measured at 150 °C on LC (a) and LCCu (b). Full symbols represent data that were considered for dispersion calculation. The total gas uptake was determined by extrapolating the straight-line portion of the adsorption isotherm to zero pressure. Symbols: (■, □) total H_2 isotherm; (●, ○) physisorbed H_2 isotherm (*i.e.*, reversible).

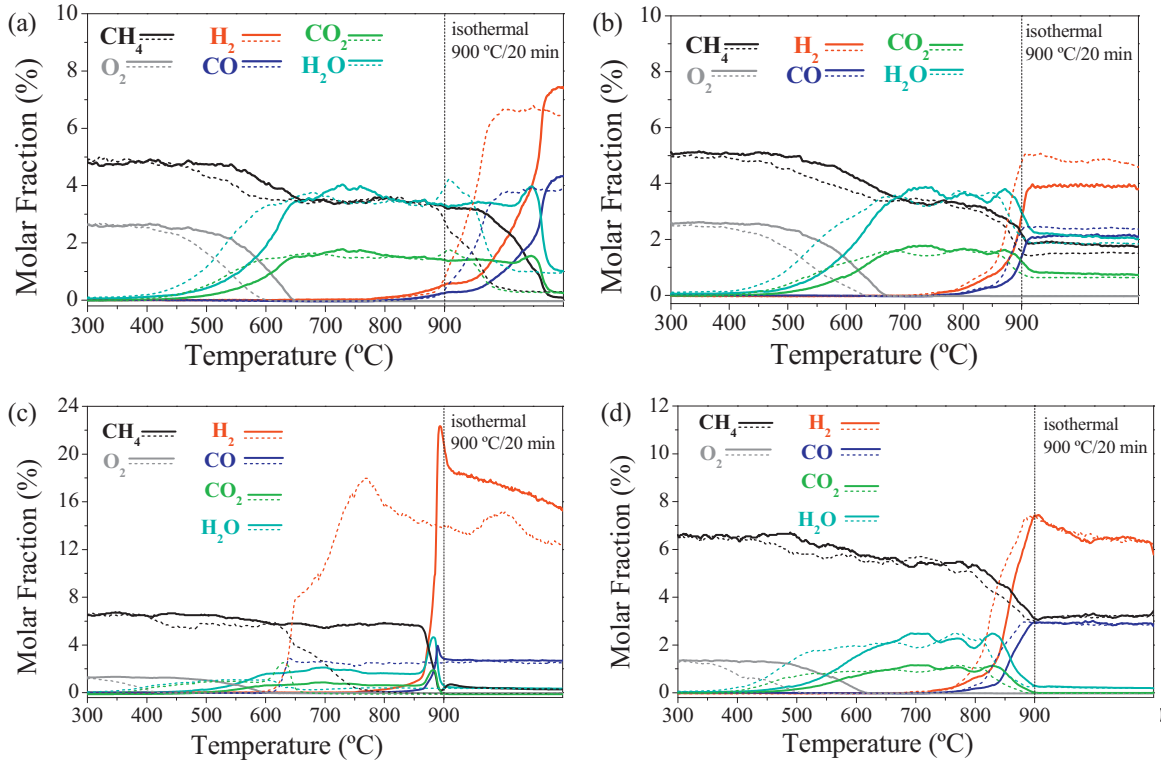

Fig. 5. Consecutive TPSR profiles of LC (a), LCCu (b) in the partial oxidation of methane $CH_4/O_2/He = 2/1/37$ and also LC (c), LCCu (d) under $CH_4/O_2/He = 5/1/64$ (10° C/min, 30 000 $cm^3\ g^{-1}\ h^{-1}$). Solid lines represent the first run and dashed lines refer to the second one.

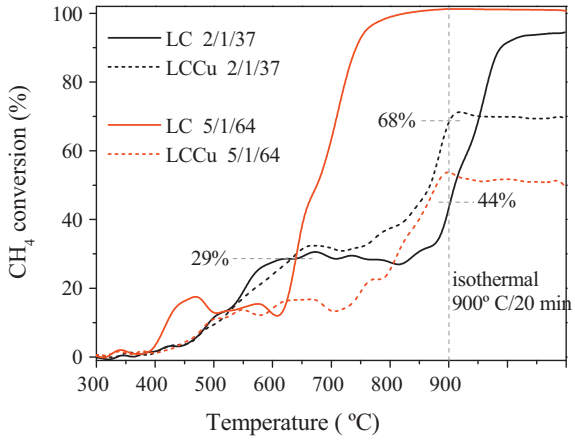

Fig. 6. Conversion of CH_4 as function of temperature for all of the catalysts in the second TPSR run. Here the solid lines refer to LC catalyst investigated under different feed streams ($CH_4/O_2/He = 2/1/37$ and 5/1/64), while dashed lines correspond to LCCu.

the second TPSR run in the POM $CH_4/O_2/He = 2/1/37$, the LCCu catalyst showed better performance than LC, *i.e.*, LCCu led to higher H_2 selectivity, lesser CO_2 formation and higher CH_4 conversions (the latter information seen in Fig. 6).

The performances of LC and LCCu catalysts in the TPSR experiments under mixture $CH_4/O_2/He = 5/1/64$ are illustrated in Figs. 5c/d. The copper-substituted catalyst presents similar behavior to that verified earlier for $CH_4/O_2/He = 2/1/37$ (see Fig. 5b and (d)); syngas arises only above 700 °C and becomes significant as the temperature increases. On the other hand, LC displays a first TPSR profile characterized by low CH_4 conversions until ~860 °C limited for low O_2 content, however the second TPSR was completely different presenting very high CH_4 conversions above 610 °C which attains approximately 100%, as well as high H_2/CO ratio and high H_2 and CO yields (Table 4). Therefore, an activation of *ca.* 230 °C for syngas production is observed from the first to the second TPSR.

If we proceed the catalytic experiments first by reducing the catalyst with H_2 and then passing the reaction mixture (*i.e.*, carry out the TPSR experiments) we obtain exactly the same profiles as those obtained without previous H_2-reduction. This situation happens because a previous H_2-reduction is annulled by O_2 reactant from the feed stream $CH_4/O_2/He = 5/1/64$ (or $CH_4/O_2/He = 2/1/37$) at the range of temperature 160–310 °C, as observed by a significant consumption of O_2 through mass spectroscopy during the first TPSR (not shown here). Since the reduced catalysts are easily reoxidized by the feed stream at temperatures <310 °C, we decided to suppress the pretreatment with H_2 and proceed with a second TPSR starting above a temperature in which the reoxidation of the metal particles (obtained in the first TPSR) is not easily promoted (*i.e.*, above 300 °C).

As shown in Fig. 5c, for example, the first TPSR without H_2 reduction showed activity only above approximately 800 °C, but in the second run (that started at 300 °C) the activity was enhanced and started at much lower temperature, *i.e.*, around 610 °C. We suggest that in the first TPSR the perovskite structure is destroyed forming cobalt oxide species which are reduced into metallic Co during the reaction above 800 °C due to formation of H_2. After this first TPSR run while the sample is cooled, the metal surface of the particles is probably reoxidized but its bulk structure possibly not, since the temperature is decreased until reaching the limit of 300 °C, below which a more complete reoxidation could take place. Therefore, as in the second TPSR only a surface CoO_x cape must be reduced to expose metallic particles, then the activity process for syngas takes place at much lower temperature. In short it means that in the first TPSR part of the H_2 product catalyzes the reduction of the oxide structure, while in the second run the preferential reduction of surface oxide cape is sufficient to initiate the reaction earlier.

Table 4
Catalytic activity in the second TPSR run (10 °C min^{-1}, 100 mg of catalyst, 30 000 cm^3 g^{-1} h^{-1}).

Catalyst	Feed stream $CH_4/H_2/He$	Temperature[a] (°C)	H_2 selectivity (%)	H_2/CO	$H_2/(CO+CO_2)$
LC	2/1/37	800	1	–[b]	0
		900	12	2.1	0.4
LCCu	2/1/37	800	6	3.5	0.2
		900	48	2.1	1.6
LC	5/1/64	600	7	4.1	0.2
		700	81	4.1	4.1
		800	87	6.5	6.5
		900	85	5.5	5.5
LCCu	5/1/64	800	25	3.6	0.9
		900	70	2.6	2.6

[a] Data at 900 °C correspond to the initial time in the isothermal plateau.
[b] CO is not produced in this condition.

TPSR profiles for LC under $CH_4/O_2/He = 5/1/64$ were similar to those observed by De Rogatis et al. [24] for a Ni/Al_2O_3 catalyst in the partial oxidation of methane $CH_4/O_2/Ar = 2/1/97$ (50 000 mL g^{-1} h^{-1}). These authors claim that there is a critical temperature at which NiO, active for total oxidation, is reduced *in situ* by methane and starts immediately to catalyze partial oxidation of methane during the second TPSR run.

In order to identify the phases existing in the spent catalysts LC and LCCu (after TPSR experiments), we carried out XRD and the diffractograms are displayed in the Figs. 7 and 8. These results indicate that after two consecutive TPSR in the POM $CH_4/O_2/He = 2/1/37$, the perovskite gives place to a complex structure composed by $La(OH)_3$, La_2O_3, La_2CoO_4, Co_3O_4, $LaCoO_3$ and CuO, the latter only in the copper-substituted catalyst (Fig. 7). The catalysts tested with the other feed stream $CH_4/O_2/He = 5/1/64$ presented $La(OH)_3$, Co and Cu, the latter existing only in the LCCu, besides Co_3O_4 which appeared only in LC (Fig. 8).

The main remarks concerning the XRD patterns are:

(i) The perovskite structure is decomposed during the temperature-programmed surface reactions basically towards lanthanum oxide and metallic species, but this transformation depends on the mixtures employed. The most reductive mixture $CH_4/O_2/He = 5/1/64$ leads to an entire structural transformation, but under $CH_4/O_2/He = 2/1/37$ some perovskite $LaCoO_3$ still remains and spinel phase La_2CoO_4 arises. A similar behavior was reported by Villoria et al. [25] after $LaCoO_3$ catalyst synthesized by Pechini method was thermal treated at 750° C in mixture containing diesel. This results are consistent with investigations that show spinels usually appear during catalytic partial oxidation conditions as reported by Vella et al. [26], in which spinel La_2NiO_4 formed from $LaNiO_3$-based catalysts and Dissanayake et al. [27], which reported the formation of $NiAl_2O_4$ from the catalyst Ni/Al_2O_3.

(ii) $La(OH)_3$ presence is ascribed to the hydration of La_2O_3 during the storage period prior the XRD analysis (the latter phase coming from the perovskite collapse in TPSR experiments). According to [28] La_2O_3 adsorbs H_2O and CO_2 when exposed to air, becoming a $La(OH)_3$ crystalline nucleus surrounded by layers of disordered $La(OH)_x(CO_3)_y$ phase. Other authors also detected the formation of $La(OH)_3$ from $LaCoO_3$ perovskite precursors and suggested that it occurs due to the hydroxylation of lanthana present in the sample upon exposure to atmospheric humidity [25] or even to the rehydration of La_2O_3 by water produced during the methane oxidation reaction [8].

(iii) The absence of metallic cobalt and copper in the catalysts investigated in the POM $CH_4/O_2/He = 2/1/37$ implies these species were probably oxidized during the storage towards Co_3O_4 and CuO;

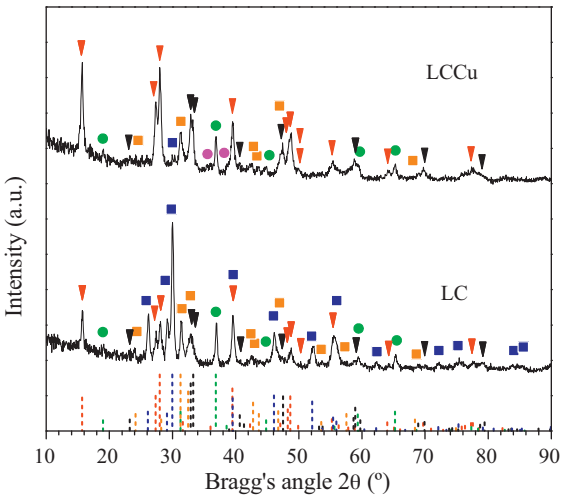

Fig. 7. Diffractograms of LC and LCCu after consecutive TPSR experiments in the partial oxidation of methane ($CH_4/O_2/He = 2/1/37$, 10 °C/min, 30 000 cm^3 g^{-1} h^{-1}). Identification: (▼) $La(OH)_3$ JCPDS 36-1481, (■) La_2O_3 JCPDS 05-0602, (▼) $LaCoO_3$ JCPDS 48-0123, (●) Co_3O_4 JCPDS 42-1467, (■) La_2CoO_4 JCPDS 34-1296 and (●) CuO JCPDS 48-1548. Dashed lines arising from the base represent the peak positions for each phase in the JCPDS patterns.

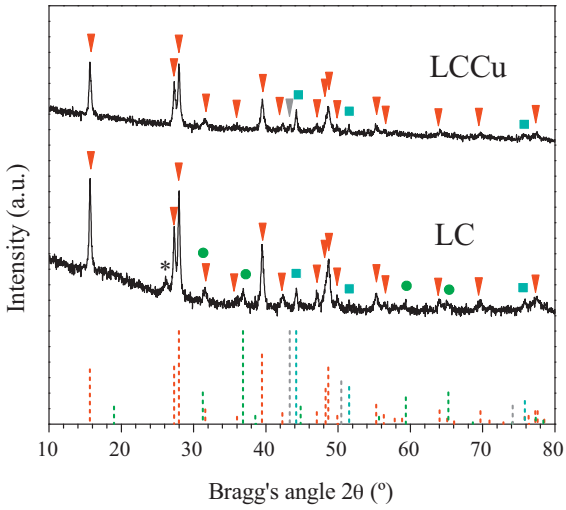

Fig. 8. Diffractograms of LC and LCCu after consecutive TPSR experiments in the $CH_4/O_2/He = 5/1/64$ mixture (10° C/min, 30 000 cm^3 g^{-1} h^{-1}). Identification: (▼) $La(OH)_3$ JCPDS 36-1481, (■) Co JCPDS 15-0806, (●) Co_3O_4 JCPDS 42-1467, (▼) Cu JCPDS 04-0836 and (*) Graphite JCPDS 41-1487. Dashed lines arising from the base represent the peak positions for each phase in the JCPDS patterns.

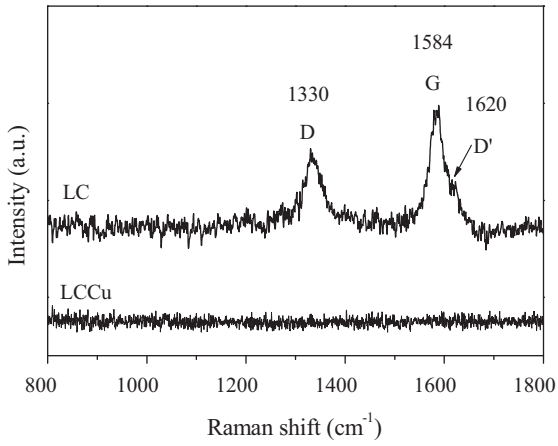

Fig. 9. Raman spectra of the LC and LCCu samples after TPSR experiments with $CH_4/O_2/He = 5/1/64$ showing characteristic features of graphitic carbon (D, G and D′ bands).

(iv) LC catalyst tested under $CH_4/O_2/He = 5/1/64$ was the unique one to present peak around $2\theta = 26.0^\circ$ referent to the plane (0 0 2) of graphite phase (JCPDS 41-1487).
(v) LCCu catalyst tested under $CH_4/O_2/He = 5/1/64$ did not present Co_3O_4, as reported with LC, which suggests that Cu modification is beneficial for preventing reoxidation of the metallic cobalt. This observation agrees with the H_2-chemisorption result which indicated that Cu promotes higher dispersion of Co when the perovskite is reduced and therefore this phenomenon may be responsible for the higher resistance of cobalt particles to reoxidize.

From the XRD data, we calculated the mean crystallite size of the metallic cobalt particles (L_{Co}). The catalysts LC and LCCu after test in the POM $CH_4/O_2/He = 5/1/64$ presented $L_{Co} = 42 \pm 14$ nm and 51 ± 13 nm, respectively, which are values with same order of magnitude of the $LaCoO_3/LaCoCuO_3$ crystallites before the reaction (Table 2). For LCCu, the peak related to metallic copper did not present enough intensity to provide reliable mean crystallite size. Therefore, the structural characterization of the catalysts after reaction by means of XRD can provide an insight on the dynamic character of the perovskite under reaction conditions. It seems to occur that the real catalyst obtained after TPSR at *ca.* 900 °C is basically metal supported on La_2O_3, therefore the performance of these perovskites can further be compared to Co and Co–Cu supported on La_2O_3 prepared by conventional methods as coprecipitation or impregnation.

In particular, for LC in the $CH_4/O_2/He = 5/1/64$ the activation process verified from the first to second TPSR run seems to be linked to an *in situ* reduction of the perovskite structure, that probably takes place in the first run but intensifies in the second one. The high ratio $4 < H_2/CO < 7.7$ observed above 700 °C indicates the occurrence of CH_4 decomposition (Eq. (1)).

$$CH_4 \leftrightarrow C + 2H_2 \rightarrow (\Delta H^0_{298\,K} = 76\,\text{kJ mol}^{-1}) \quad (1)$$

This reaction leads to carbon deposition as confirmed by XRD (presence of graphite phase). This result agrees with the Raman spectroscopy for this sample after the test (Fig. 9), which showed bands at 1330 and 1584 cm^{-1} (D and G bands, respectively) and a small shoulder at 1620 cm^{-1}, all of them related to carbon filaments [29]. All allotropic forms of carbon, *e.g.*, fullerenes, carbon nanotubes, amorphous carbon, polycrystalline carbon, are active in Raman spectroscopy [30] and the position, width and relative intensity of bands are modified according to the carbon forms [31]. The most characteristic features are a large structure (1340 cm^{-1}) assigned to residual ill-organized graphite, the so-called D-line (D: disorder); a high-frequency bunch (between 1500 and 1600 cm^{-1}) called G band also characteristic of nanotubes, corresponding to a splitting of the E_{2g} stretching mode of graphite [32]; and a weak band around 1618 cm^{-1} called D' and typical of defective graphitic material.

SEM images proved the catalyst surface was covered by carbon filaments after the TPSR under $CH_4/O_2/He = 5/1/64$, as shown in Fig. 10a. TEM images still showed many metal particles carried inside the carbon nanotubes like those pointed out in the white circles in Fig. 10b. In this same picture, a free metal particle is situated close to the upper extremity of the nanotube, probably acting as a site for reactions like CH_4 decomposition, partial oxidation and reforming of CH_4.

The collapse of the perovskite structure of LC started probably during the first TPSR run towards the formation of Co^0, carbon and La_2O_3. At temperatures as high as 900 °C, metallic cobalt was expected to be formed, due the reductive atmosphere. Afterwards, in the consecutive run (that initiated at 300 °C) the reaction mixture met a more reduced and favorable surface for methane decomposition. Increasing the temperature, the products H_2O and CO_2 also started to be consumed, suggesting that steam reforming and dry reforming of methane had important role in the set of reactions (above 630 °C in Fig. 5c). In addition, other reactions such as Boudouard reaction (Eq. (2)) could increase the carbon deposition, supplying CO_2 for the dry reforming.

$$2CO \leftrightarrow C + CO_2 \rightarrow (\Delta H^0_{298\,K} = 76\,\text{kJ mol}^{-1}) \quad (2)$$

The copper-substituted catalyst (LCCu) tested in the mixture $CH_4/O_2/He = 5/1/64$ presented a slight activation for syngas production from the first to the second TPSR run (Fig. 5d), which is also ascribed to the reduction of perovskite. The diffractogram of LCCu after reaction showed collapse of the oxide structure and formation of metallic copper and cobalt but absence of graphitic phase. Raman spectroscopy did not indicate presence of any band related to carbon filaments as shown in Fig. 9, and no carbon structures were evidenced by SEM analysis, suggesting that copper inhibits carbon deposition efficiently, although amorphous carbon in a small extent cannot be discarded. However, SEM allowed identifying many spherical particles with large diameter distribution over the entire surface of the spent LCCu catalyst, as viewed in Fig. 10c and d. The EDS mapping on this catalyst showed homogeneous distribution of copper but slight concentration of cobalt over the spherical particles seen in the micrographs. EDS microanalysis carried out specifically on these particles provided a ratio $1.8 < Co/La < 2.6$, suggesting that these particles are metallic cobalt originated from reduction of the perovskite structure since the nominal ratio Co/La = 0.8 and the distribution of Co, Cu and La elements on the surface before the reaction was very homogeneous, as indicated by the EDS mapping.

The TPSR profiles obtained for LCCu under both mixtures $CH_4/O_2/He = 2/1/37$ and $5/1/64$ were similar to those observed by [24] for 10% Cu/Al_2O_3 in the partial oxidation of methane $CH_4/O_2/Ar = 2/1/97$ (50 000 mL g^{-1} h^{-1}). In both cases there was low methane conversion and predominance of total oxidation up to 800 °C. However, the presence of copper in the perovskite catalyst investigated in this work had a very important impact over the CH_4 decomposition: while LC presented wide carbon nanotube presence after tests with $CH_4/O_2/He = 5/1/64$, LCCu containing only 5.2 wt.% of Cu was able to inhibit carbon deposition. According to Twigg and Spencer [33], unlike reactions involving transition metal catalysts such as those containing iron, nickel or cobalt, copper catalysts have no strong tendency to catalyze Fisher–Tropsch reactions or processes involving carbonium ion chemistry, which can give rise to various possible precursors of carbonaceous deposits. Copper also has a very low activity for breaking C–O bonds or for

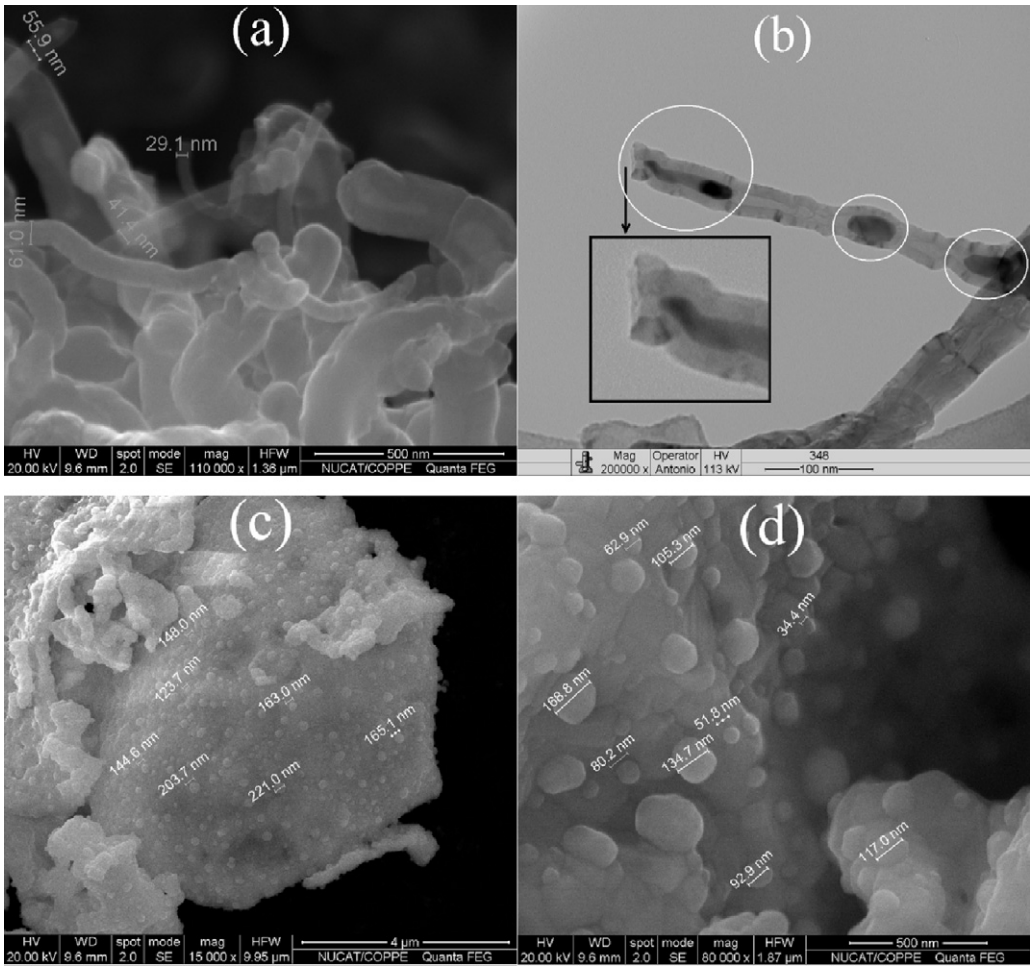

Fig. 10. Micrographs of LC (a, b) and LCCu (c, d) catalysts after consecutive TPSR experiments under $CH_4/O_2/He = 5/1/64$ mixture. Image (b) was obtained by TEM, while other images by SEM.

forming C–C bonds, and thus wax formation is not usually a major problem in CO/H_2 reactions, nor coke formation from any hydrocarbons present.

Copper-substituted materials have been widely investigated in the literature, not only in perovskite oxides but also in other bimetallic systems. Lee et al. [34,35] have studied bimetallic Co–Cu systems for direct use of hydrocarbons in solid oxide fuel cells and stated that changes in physico-chemical and catalytic properties, due to the copper presence, are advantageous in their application as oxidation catalysts, especially for modifying the mechanism through which carbon is formed on the active sites. Temperature-programmed oxidation demonstrated the anode containing bimetallic $Cu_{0.1}Co_{0.9}$ was significantly more resistant to coke deposition (5 wt.% of carbon) than the system without copper (>200 wt.%) [35]. Besides avoiding carbon formation, copper insertion into the lattice of the catalyst can influence its stability and redox properties as evidenced by Tien-Thao et al. [11] when investigating the copper-doped $LaCoO_3$ perovskites applied in the synthesis of higher alcohols. These authors concluded that strong cobalt–copper interaction in perovskites could enhance the metallic dispersion of cobalt and prevent copper sintering.

In the present work, the H_2-TPR results (Fig. 3) showed that Cu modified the reducibility of the perovskite structure decreasing the maximum temperature of the reduction peaks by approximately 60 °C. The beneficial interaction between copper–cobalt under reducing conditions was clearly verified with H_2-chemisorption that showed a significant increase of H_2-uptake when copper is present, even in low content.

TGA analysis was carried out with the samples after TPSR experiments in order to quantify the mass associated to carbon on the catalysts. The results are depicted in Fig. 11. For all of the catalysts a first step can be viewed in between 200 and 350 °C, corresponding to a loss of 3.3–4.6 wt.% attributed to H_2O and CO_2 released from

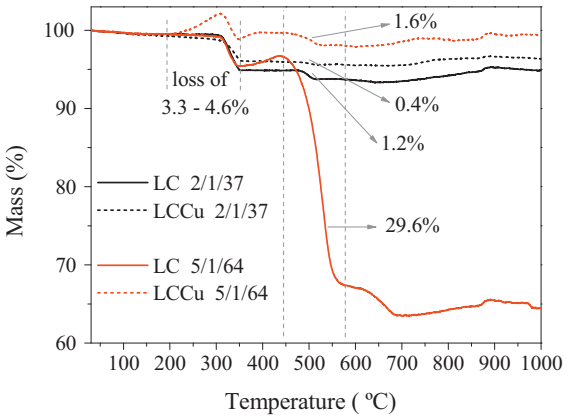

Fig. 11. TGA curves of the catalysts after consecutive TPSR experiments. Solid lines refer to LC catalyst investigated under different feed streams ($CH_4/O_2/He = 2/1/37$ and 5/1/64), while dashed lines correspond to LCCu.

the decomposition of $La(OH)_3$ and $La(OH)_x(CO_3)_y$, according to the scheme [28,36]:

$$\begin{matrix} La(OH)_3 \\ La(OH)_x(CO_3)_y \end{matrix} \rightarrow \begin{matrix} LaO(OH) \\ La_2(OH)_2CO_3 \end{matrix} + H_2O \rightarrow \begin{matrix} La_2O_3 \\ La_2O_2CO_3 \end{matrix} + H_2O \rightarrow La_2O_3 + CO_2$$

Afterwards a second step of mass loss related to carbon occurs above ~450 °C and finishes at different temperatures for each catalyst. The extension of this second stage is associated to the amount of coke and/or carbon filaments present on the catalyst surface. LC and LCCu after POM $CH_4/O_2/He = 2/1/37$ (black lines in Fig. 11) showed loss of 1.2 and 0.4 wt.%, respectively, in between 460 and 650 °C. Although the micrographs and Raman spectroscopy (not shown here for the catalysts after POM $CH_4/O_2/He = 2/1/37$ because no band associated to graphite was detected), and XRD patterns have not shown evidence to the presence of carbon filaments on LC and LCCu, the mass loss is associated to the presence of coke. The lowest percentage presented by LCCu (0.4 wt.%) indicates that copper was able to suppress coke formation when compared to LC.

On the other hand, the catalysts tested under $CH_4/O_2/He = 5/1/64$ (red lines) presented higher mass loss. LC lost 29.6 wt.% in mass which can be associated to carbon nanotubes and carbon nanofibers as identified using electronic microscopy (Fig. 10a and b). The decrease of mass occurring up to ~700 °C (the highest temperature for all the experiments) is ascribed to the high thermal resistance of multi-wall carbon nanotubes and nanofibers; the former usually resists until 650 °C under air flow but the latter can reach 900 °C [37]. Contrasting to LC, the copper-substituted catalyst was more efficient for suppressing carbon deposition and the mass loss was indicated to be 1.6%, *i.e.*, 18.5 times less than observed for LC. When comparing micrographs Fig. 10a–d and taking into account the TGA result, it is clear that the copper presence has a decisive role in the catalyst for suppressing carbon deposition and avoid quick deactivation, since a reactor with LC would have an unavoidable clogging over time, while LCCu would have more time to operate if the experiment was maintained or more cycles were done.

An important remark to be pointed out at the TGA profiles is the gain of mass observed at low (<500 ° C) and high (>700 °C) temperatures. Since LC and LCCu catalysts tested in TPSR under $CH_4/O_2/He = 5/1/64$ were the only materials to present metallic phase at the occasion of the XRD and TGA analysis, the increase of mass observed for this catalysts at low temperatures (and only for them) is ascribed to the reoxidation of metallic copper and cobalt species. This gain of mass corresponded to 1.4 and 2.8% for LC and LCCu, respectively, but subsequently the mass decreased due to carbon elimination as CO_2. Meanwhile, the gain of mass above 700 °C observed for all the catalysts, varying from 1.4 to 2.2%, is attributed to a partial reoxidation of the perovskite structure, since perovskite oxides may be reversible reduced and reoxidized whether a strong sintering of phases does not take place [38]. Provendier et al. [2], for instance, have proved that partially reduced $LaNi_xFe_{1-x}O_3$ ($x < 0.4$) perovskites were able to recover the initial structure after a simple calcination step and Viparelli et al. [39] showed that $Ba(ZrRh)O_3$ perovskites presented a redox cycle when alternating reducing and oxidizing atmospheres under temperature programmed heating up to 1250 ° C, with partial reincorporation of rhodium into the re-established perovskite structure. Similar interpretation to the TGA curves was obtained by [25,26] concerning the reoxidation of metallic Ni or Co in spent $LaCoO_3$ and $LaNiCoO_3$ catalysts.

The thermogravimetric analysis carried out in the present work provided a quantitative view about the previous evidences obtained with XRD, Raman spectroscopy and microscopy: copper-doped $LaCoO_3$ is significantly more resistant against carbon deposition than $LaCoO_3$ and this may extend its application as catalyst to many reactions dealing with hydrocarbons.

4. Conclusions

This article presents a study on the structural transformations of $LaCoO_3$ and $LaCoCuO_3$ catalysts tested in the partial oxidation of methane in transient experiments through a large range of temperature. The perovskite-type oxides were synthesized by the polymerizable complex route and this methodology showed to be suitable for obtaining catalysts with single phase and copper substitution into the B-site of the perovskite. The characterizations performed before and after temperature-programmed surface reactions indicated a collapse of the oxide structure of $LaCoO_3$ and $LaCoCuO_3$ towards a lanthanum-based matrix and metal cobalt and copper, but extent of this collapse depended on the reaction mixture employed for the experiment, *i.e.*, the more reducing atmosphere $CH_4/O_2 = 5/1$ was able to reduce completely the perovskite structure after two consecutive temperature-programmed runs, but under $CH_4/O_2 = 2/1$ some perovskite remained.

High activity to syngas was observed for $LaCoO_3$ catalyst under $CH_4/O_2 = 5/1$ but it was caused by methane decomposition, which is responsible for a significant formation of carbon filaments and consequently deactivation of the catalyst. On the other hand, the copper-substitution in the perovskite lattice led to a catalyst able to produce syngas above 800 °C and with good resistance to carbon deposition in both reaction mixtures $CH_4/O_2 = 2/1$ and 5/1. In short, effects of copper addition include carbon inhibition on the catalyst, increase of reducibility and decrease of temperature to obtain syngas. Copper may be a very important dopant for perovskites applied in reactions with hydrocarbons.

Acknowledgments

The authors acknowledge Dr. Marta C. Amorim for SEM analysis; CNPq, CAPES, FAPERJ and FINEP for financial support and Universidade Santa Úrsula – Rio de Janeiro/Brazil for TEM analysis.

References

[1] D. Ferri, L. Forni, Appl. Catal. B 16 (1998) 119–126.
[2] H. Provendier, C. Petit, C. Estournès, S. Libs, A. Kiennemann, Appl. Catal. A 180 (1999) 163–173.
[3] M.R. Goldwasser, M.E. Rivas, M.L. Lugo, E. Pietri, J. Pérez-Zurita, M.L. Cubeiro, A. Griboval-Constant, G. Leclercq, Catal. Today 107–108 (2005) 106–113.
[4] B. Echchahed, S. Kaliaguine, H. Alamdari, Int. J. Chem. Reactor Eng. 4 (2006) A29.
[5] A. Slagtern, U. Olsbye, Appl. Catal. A 110 (1994) 99–108.
[6] R. Lago, G. Bini, M.A. Peña, J.L.G. Fierro, J. Catal. 167 (1997) 198–209.
[7] G.C. Araujo, S. Lima, M.C. Rangel, V. La Parola, M.A. Peña, J.L.G. Fierro, Catal. Today 107–108 (2005) 906–912.
[8] C.R.B. Silva, L. Conceição, N.F.P. Ribeiro, M.M.V.M. Souza, Catal. Commun. 12 (2011) 665–668.
[9] G.L. Chiarello, J.D. Grunwaldt, D. Ferri, J. Catal. 252 (2007) 127–136.
[10] N. Mota, R.M. Navarro, M.C. Alvarez-Galvan, S.M. Al-Zahrani, J.L.G. Fierro, J. Power Sources 196 (2011) 9087–9095.
[11] N. Tien-Thao, H. Alamdari, M.H. Zahedi-Niaki, S. Kaliaguine, Appl. Catal. A 311 (2006) 204–212.
[12] J.A. Villoria, M.C. Alvarez-Galvan, R.M. Navarro, Y. Briceño, F. Gordillo Alvarez, F. Rosa, J.L.G. Fierro, Catal. Today 138 (2008) 135–140.
[13] M. Popa, M. Kakihana, Solid State Ionics 151 (2002) 251–257.
[14] M. Popa, J.M. Calderon-Moreno, J. Eur. Ceram. Soc. 29 (2009) 2281–2287.
[15] M. Kumar, S. Srikanth, B. Ravikumar, T.C. Alex, S.K. Das, Mater. Chem. Phys. 113 (2009) 803–815.
[16] R.C. Reuel, C.H. Bartholomew, J. Catal. 85 (1984) 63–77.
[17] J. Xiong, Ø. Borg, E.A. Blekkan, A. Holmen, Catal. Commun. 9 (2008) 2327–2330.
[18] R.R.C.M. Silva, M. Schmal, R. Frety, J.A. Dalmon, J. Chem. Soc. Faraday Trans. 89 (1993) 3975–3980.
[19] R.D. Shannon, Acta Crystallogr. A 32 (1976) 751–767.
[20] P. Porta, S. Rossi, M. Faticanti, G. Minelli, I. Pettiti, L. Lisi, M. Turco, J. Solid State Chem. 146 (1999) 291–304.
[21] G. Leofanti, M. Padovan, G. Tozzola, B. Venturelli, Catal. Today 41 (1998) 207–219.
[22] L. Bedel, A.C. Roger, C. Estournes, A. Kiennemann, Catal. Today 85 (2003) 207–218.
[23] J.L. Figueiredo, F.R. Ribeiro, Catálise Heterogênea, Fundação Calouste Gulbenkian, Lisboa, 1987, pp. 166–168.

[24] L. De Rogatis, T. Montini, A. Cognigni, L. Olivi, P. Fornasiero, Catal. Today 145 (2009) 176–185.
[25] J.A. Villoria, M.C. Alvarez-Galvan, S.M. Al-Zahrani, P. Palmisano, S. Specchia, V. Specchia, J.L.G. Fierro, R.M. Navarro, Appl. Catal. B 105 (2011) 276–288.
[26] L.D. Vella, J.A. Villoria, S. Specchia, N. Mota, J.L.G. Fierro, V. Specchia, Catal. Today 171 (2011) 84–96.
[27] D. Dissanayake, M.P. Rosynek, K.C.C. Kharas, J.H. Lunsford, J. Catal. 132 (1991) 117–127.
[28] A. Galtayries, G. Blanco, G.A. Cifredo, D. Finol, J.M. Gatica, J.M. Pintado, H. Vidal, R. Sporken, S. Bernal, Surf. Interface Anal. 27 (1999) 941–949.
[29] T. Belin, F. Epron, Mater. Sci. Eng. B 119 (2005) 105–118.
[30] S. Arepalli, P. Nikolaev, O. Gorelik, V. Hadjiev, W. Holmes, B. Files, L. Yowell, Carbon 42 (2004) 1783–1791.
[31] A. Ferrari, J. Robertson, Phys. Rev. B 61 (2000) 14095–14107.
[32] A.A. Mamedov, N.A. Kotov, M. Prato, D.M. Guldi, J.P. Wicksted, A. Hirsch, Nat. Mater. 1 (2002) 190–194.
[33] M.V. Twigg, M.S. Spencer, Top. Catal. 22 (2003) 191–203.
[34] S.I. Lee, J.M. Vohs, R.J. Gorte, J. Electrochem. Soc. 151 (2004) A1319–A1323.
[35] S.I. Lee, K. Ahn, J.M. Vohs, R.J. Gorte, Electroch. Solid St. 8 (2005) A48–A51.
[36] R.M. Navarro, M.C. Alvarez-Galvan, J.A. Villoria, I.D. González-Jiménez, F. Rosa, J.L.G. Fierro, Appl. Catal. B 73 (2007) 247–258.
[37] P. Serp, M. Corrias, P. Kalck, Appl. Catal. A 253 (2003) 337–358.
[38] M.A. Peña, J.L.G. Fierro, Chem. Rev. 101 (2001) 1981–2017.
[39] P. Viparelli, P. Villa, F. Basile, F. Trifirò, A. Vaccari, P. Nanni, M. Viviani, Appl. Catal. A 280 (2005) 225–232.